J Appl Electrochem (2014) 44:953–962
DOI 10.1007/s10800-014-0704-0

RESEARCH ARTICLE

Nanostructured manganese oxide–chitosan-based cholesterol sensor

Chumki Charan · Vinod K. Shahi

Received: 4 April 2014 / Accepted: 9 June 2014 / Published online: 28 June 2014

Abstract Manganese oxide nano-rod (nano-MnO_2) was prepared by simple oxidation method. To fabricate nanocomposite film (nano-MnO_2/CT) onto glassy carbon electrode (GCE), nano-MnO_2 was homogeneously dispersed in chitosan (CT). Cholesterol oxidase (ChOx) was immobilized onto nano-MnO_2/CT by physisorption. Modified electrode was characterized by Fourier transform infrared, X-ray diffraction, cyclic voltammetry, scanning electron microscopy, transmission electron microscopy, and electrochemical impedance spectroscopy techniques. Prepared ChOx/nano-MnO_2/CT/GCE bioelectrode exhibited 0.03–11.66 mM linearity and 2.07×10^{-3} mM limit of detection for cholesterol. Biosensing characteristics of modified bioelectrode were superior than other electrodes modified with metal oxide nanoparticles, reported in the literature.

Keywords Cholesterol detection · Biosensor · Manganese oxide nanoparticles · Electrochemical biosensor

1 Introduction

Cholesterol is a waxy steroid metabolite and presents in the cell membranes and blood plasma [1, 2]. It is an important component for the manufacture of bile acids, steroid hormones, and fat soluble vitamins (vitamin A, vitamin D, vitamin E, and vitamin K). High concentration level of serum cholesterol is an indicator for diseases such as hypertension, myocardial infarction, and arteriosclerosis. Cholesterol concentration in the blood is an important parameter to diagnose or prevent these diseases. Thus, development of a cholesterol biosensor with high sensitivity, easy operation, and low cost is important.

For cholesterol detection, available biochemical tests and sensors are expensive, slow, insensitive, and non-specific [3]. Electrochemical biosensors (ECB) are effective tool for the analysis of biological molecules, because of their simplicity, quick, inexpensive, portable nature, and reliable response over wide concentration range. But immobilization of enzyme (ChOx) onto an electrode surface is a critical step to obtain desired biosensing characteristics. Thus, development of new material with biocompatibility and selectivity is essential for designing cholesterol biosensor [3–7].

CT is an interesting biopolymer, and contains amino groups, which provides hydrophilic environment for biomolecules interactions [8, 9]. Several research works were devoted to utilize biosensor applications of CT. These include structural modification, adjustment of molecular factors, and incorporation of metal oxide nanoparticles [4, 5, 10, 11]. Metal oxide nanoparticle-based analytical devices are cost-effective, highly sensitive (large surface-to-volume ratio), and providing excellent selectivity for bio-recognition [12–15]. Different metal oxide nanoparticles, such as ZnO [6], Fe_3O_4 [16, 17], SnO_2 [18], TiO_2 [19], ZrO_2 [20], and CeO_2 [21, 22], were screened for biosensor application. Metal oxide–CT-based cholesterol biosensors were suffered due to low efficiency, interferences, and high cost [7, 23–28]. Electrode modified with MnO_2 nanoparticles blended Nafion containing multiwall

C. Charan · V. K. Shahi
Academy of Scientific and Innovative Research, New Delhi, India

C. Charan · V. K. Shahi (✉)
Electro-Membrane Processes Division, CSIR-Central Salt and Marine Chemicals Research Institute, G.B. Marg, Bhavnagar 364002, Gujarat, India
e-mail: vkshahi@csmcri.org; vinodshahi1@yahoo.com

carbon nanotube and immobilized with ChOx showed 1–100 nM linear response with 0.3 nM cholesterol detection limits under optimum conditions [29]. But no study was conducted on the effect of interferents, as in real blood and food samples. Thus, it is necessary to develop cholesterol biosensor for its detection in less than 5.2 mM concentration in the presence of different interferents [30]. MnO_2 powder is unstable, migrated from enzyme layer, and decomposed by hydrogen peroxide [29, 31]. To overcome above-mentioned problems and exploit biosensing properties, development of stable nanostructured MnO_2 is necessary. Herein, we are reporting ChOx/nano-MnO_2/CT/GCE nanostructured biosensor for rapid and sensitive detection of cholesterol with high accuracy.

2 Materials and methods

2.1 Materials

Chitosan (high molecular weight and ≥75 % of degree of deacetylation) and cholesterol oxidase (EC 1.1.36 from *Pseudomonas fluorescences*; specific activity: 24 U mg^{-1}) were obtained from Sigma-Aldrich. Dextrose, ascorbic acid (AA), urea, and uric acid (UA) were purchased from Fluka Chemicals. Ammonium persulfate, triton X-100, phosphate buffer pellets, sodium hydroxide, and hydrochloric acid of analytical grade were obtained from S. D. Fine Chemicals, India. Double distilled water was used for the experiments.

2.2 Preparation of cholesterol solution and nano-MnO_2

The stock solution of ChOx (1 mg dl^{-1}) was freshly prepared in phosphate buffer (50 mM) at pH: 7.0. The stock solution of cholesterol was prepared in 10 % triton X-100 and stored at 4 °C. To synthesize MnO_2, separate solutions of $MnSO_4.H_2O$ (0.008 mol) and $(NH_4)_2S_2O_8$ (oxidizing agent; 0.007 mol) were prepared in water at room temperature [32]. Their equal volumes (13.5 ml, each) were mixed and transferred into a 40 ml Teflon-lined stainless steel autoclave, sealed, and maintained at 140 °C for 12 h. Impurities of the reaction product (solid) were removed by washing with distilled water. The whole reaction may be written as

$$MnSO_4 + (NH_4)S_2O_8 + 2H_2O \rightarrow MnO_2 + (NH_4)_2SO_4 + 2H_2SO_4 \quad (1)$$

2.3 Fabrication of ChOx–nano-MnO_2–CT/GC bioelectrode for cholesterol sensor

For the preparation of bioelectrode, chitosan flakes (0.5 wt%) were dissolved in 0.05 M acetate buffer solution (10 ml) and kept overnight at room temperature. MnO_2 nanoparticles (10 mg) were dispersed under continuous stirring (30 min) and sonication (1 h) at 27 °C. Glassy carbon electrode (GCE; 7.07 mm^2) was rinsed with Milli-Q water for 5–10 min and ultra sonicated in nitric acid (1:1), acetone followed by redistilled water (10 min each). Above prepared suspension (10 µl) was carefully coated on cleaned GCE and dried to obtain nano-MnO_2/CT/GCE. Modified GCE electrode was washed with deionized water followed by phosphate buffer (50 mM, pH: 7.0). For a comparative study, pristine CT/GC electrode was also fabricated. Freshly prepared 10 µl ChOx solution (1 mg ml^{-1}) was dropped onto modified and pristine GCE electrode, and stored at 4 °C for 12 h. Obtained bioelectrode was immersed in 50 mM PBS (pH 7.0) to remove excess of ChOx.

2.4 Instruments

FT-IR spectra were recorded by KBr technique in the range of 400–4,000 cm^{-1} with spectrum GX series 49387 spectrometer. For scanning electron microscopy (SEM), gold sputter coatings were carried out on the composite film at 0.1–1.0 Pa pressure and images were recorded at 10^{-3}–10^{-2} Pa EHT 15.00 kV with 300 V collector bias using Leo microscope. Electrochemical experiments were performed with potentiostat/galvanostat (Autolab® PGSTAT-302 N, Eco Chemie B.V., The Netherlands). A conventional three electrodes cell assembly containing modified (ChOx/Nano-MnO_2/CT/GC) or pristine (ChOx/CT/GC) bioelectrode as working electrode was used for electrochemical measurements. Saturated calomel electrode (SCE) and platinum wire were used as reference and counter electrodes, respectively. All the electrochemical characterizations were carried out in PBS (50 mM, pH 7.0, 0.9 NaCl) containing $[Fe(CN)_6]^{3-/4-}$.

3 Results and discussion

3.1 Characterizations of nano-MnO_2/CT

FTIR spectra of MnO_2 did not show any peak (Fig. 1). In case of CT, bands for amino saccharide aroused at 3,200–3,400 cm^{-1} (overlapping of OH and NH_2 groups) (Fig. 1). A peak at 1,650 cm^{-1} was attributed to amide group (C–O stretching along with N–H deformation mode), and band at 1,540 cm^{-1} confirmed presence of NH_2 group. The peaks at 1,425, 1,340, and 1,151 cm^{-1} were assigned to C–N band (amino group band), –COO group (carboxylic acid salt), and glucosidic linkage of polysaccharide unit, respectively [3]. Absorptions at 1,080 and 1,028 cm^{-1} aroused due to the stretching vibrations of hydroxyl and C–O–C group in glucose circle [16]. FTIR spectra of MnO_2/CT nanocomposite showed all the characteristic bands for CT and MnO_2 nanoparticles [16]. In nanocomposite, stretching vibrations shifted toward low wave number for

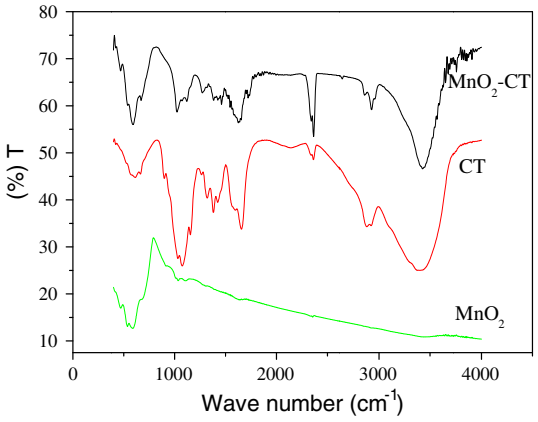

Fig. 1 FTIR spectra of CT, Nano-MnO_2, and Nano-MnO_2/CT

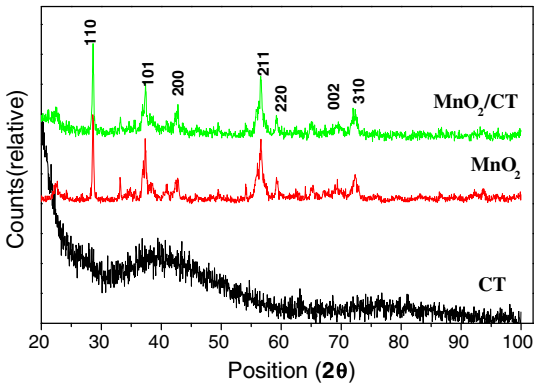

Fig. 2 XRD of CT, Nano-MnO_2, and Nano-MnO_2/CT

amino and hydroxyl groups. The peaks at 1,025, 656, and 617 cm^{-1} in the spectra of MnO_2/CT were assigned to H-bonding between Mn–O with –OH [33]. Thus, the formation of MnO_2/CT nanocomposite by H-bonding was successfully achieved.

Nano-MnO_2 was prepared by the hydrothermal method, and XRD profile of nano-MnO_2/CT (Fig. 2) showed peaks at $2\theta = 33.2°$, 37.4°, 42.8°, 56.5°, 59.2°, 64.8°, 69.0°, and 72.3° due to the Bragg reflections corresponding to the [110], [101], [200], [210], [211], [220], [002], and [310] sets of lattice planes [34]. This was similar to β-MnO_2 pattern. All the diffraction peaks were indexed as tetragonal phase β-MnO_2 and consistent with the values reported in the literature (JCPDS 24-0735) [34]. CT showed broad peak at $2\theta = 30$–50° indicates the amorphous nature. Based on these studies, schematic diagram for the fabrication of bioelectrode was depicted in Fig. 3.

3.2 Microscopy studies of MnO_2/CT nanocomposite

SEM image for CT showed homogeneous surface (Fig. 4a), whereas, MnO_2 was rod shaped (Fig. 4b). MnO_2/CT exhibited layered morphology containing MnO_2 particle compressed in CT (Fig. 4c). Further, SEM images confirmed homogeneous dispersion of MnO_2 nanoparticles in CT.

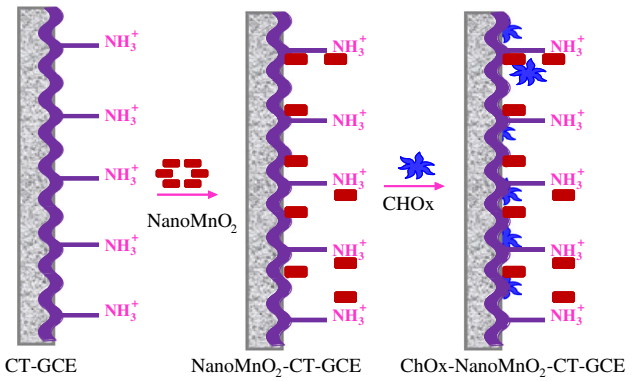

Fig. 3 Schematic diagram for the preparation of ChOx/Nano-MnO_2/CT/GCE bioelectrode

Shape and size of MnO_2 nanoparticles and MnO_2/CT were analyzed by TEM images. Nano-rod-shaped MnO_2 showed around 200–350 nm 1D rod length (Fig. 4d), while MnO_2/CT exhibited about 20–50 nm nano-rod diameter (Fig. 4e–h). Further, thick and bright spots (aroused due to electron diffraction of metal oxide particles) were assigned to the aggregation of nanoparticles (Fig. 4i). Selected area electron diffraction (SAED) images were identified as [110] and [200] planes of MnO_2 [34]. Shape of the MnO_2 plays an important role. 1-D nano structure of the MnO_2 possesses high surface area, short distance from surface to interior core, and smallest dimension, which will provide more effective electrical transport continuity, minimize diffusion path, and enhance the diffusion rate.

3.3 Electrochemical response of cholesterol

Surface resistivity as a function of frequency was measured by impedance spectra, for CT/GCE and nano-MnO_2/CT/GCE electrode with and without ChOx immobilization. Nyquist plots (Fig. 5) confirmed relatively high resistance of ChOx-modified bioelectrode in compare with the unmodified electrode. This was attributed to the insulating layers at the electrode/electrolyte interface. Immobilization of ChOx onto electrode surface was expected to hinder the electron transfer, and thus enhanced the resistance. Amount of nano-MnO_2 in ChOx/nano-MnO2/CT/GCE bioelectrode affected the detection performance for cholesterol. Thus, amount of nano-MnO_2 in the chitosan was optimized and 10 mg of nano-MnO_2 loading in 10 ml chitosan solution exhibited best result.

Electrochemical response of cholesterol was investigated by cyclic voltammograms (CVs). CVs of CT and

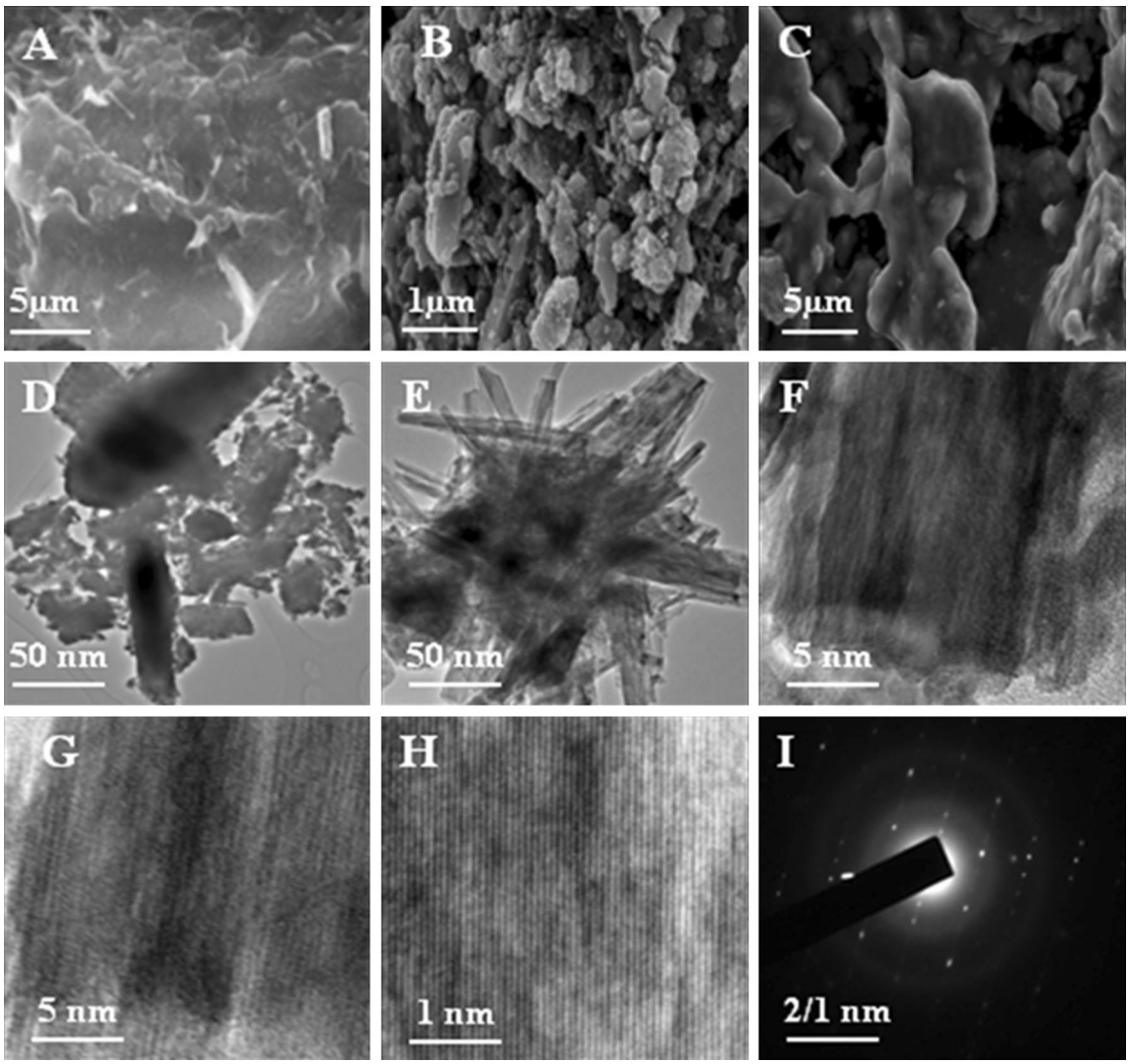

Fig. 4 SEM images of **a** CT, **b** Nano-MnO_2, and **c** Nano-MnO_2/CT; TEM images of **d** Nano-MnO_2, **e** Nano-MnO_2/CT, and **e**–**h** Nano-MnO_2/CT at different magnification; and **i** SAED picture of the Nano-MnO_2/CT

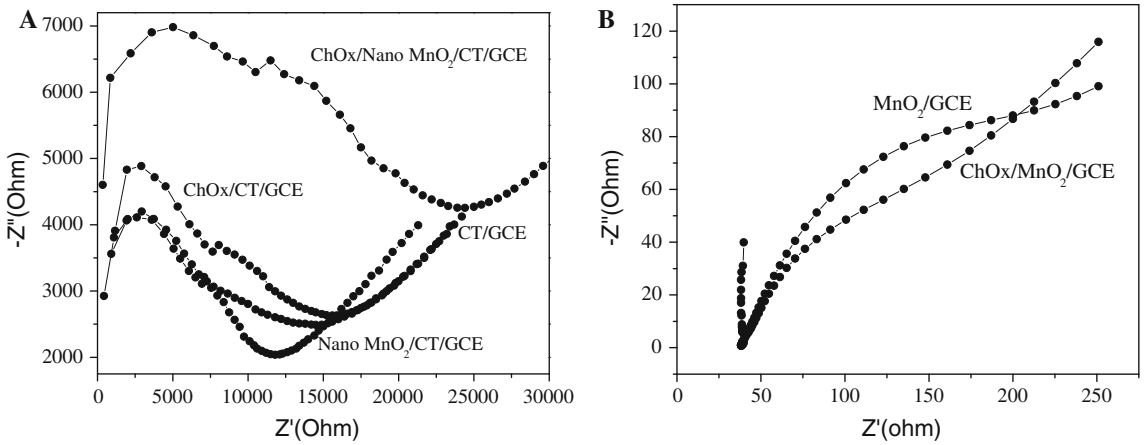

Fig. 5 **a**, **b** EIS of different modified electrodes in PBS (50 mM, pH 7.0, 0.9 % NaCl) containing 5 mM $[Fe(CN)_6]^{-3/-4}$

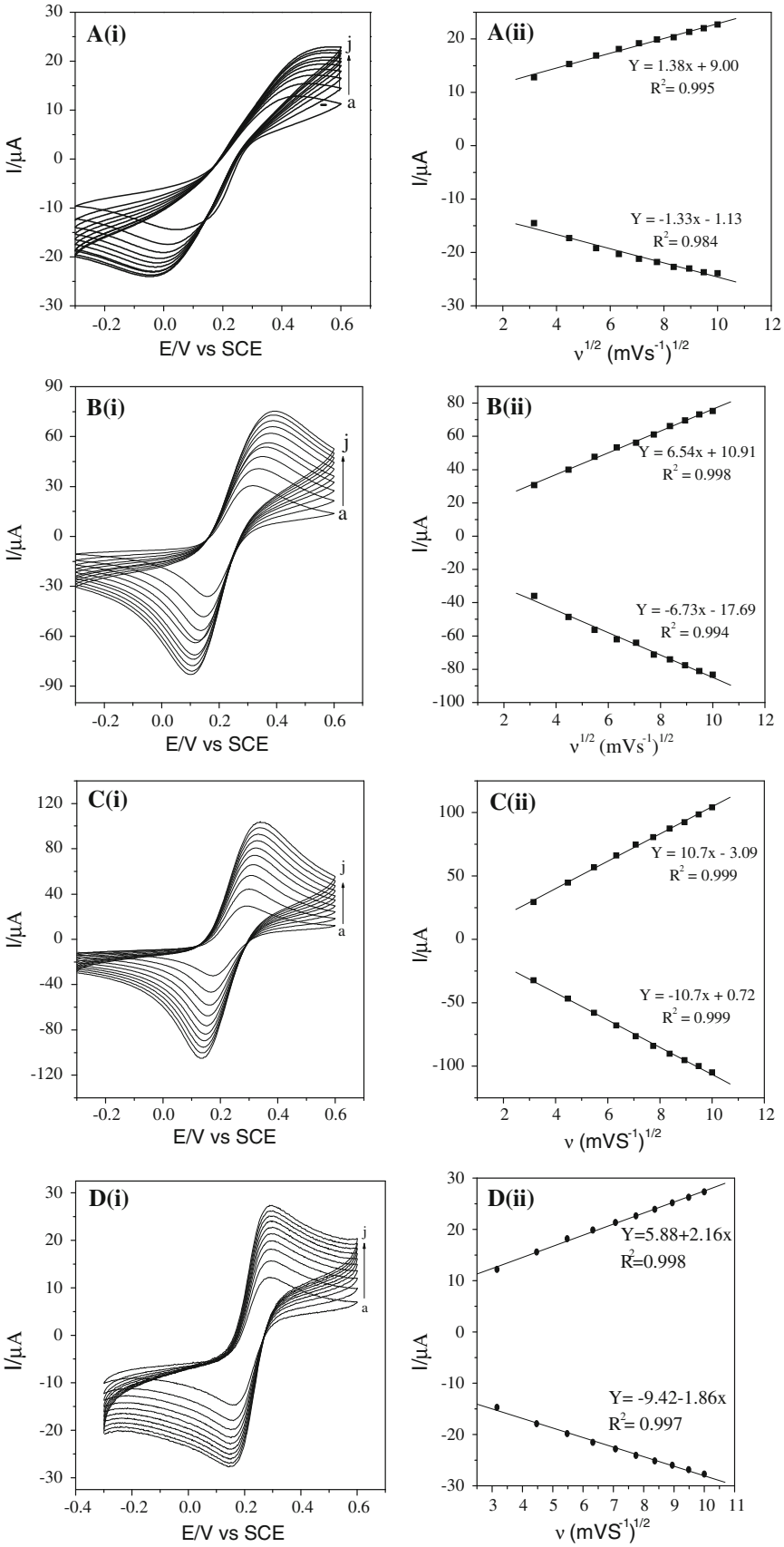

Fig. 6 CVs of *i* at different scan rate and *ii* anodic and cathodic peak currents and square root of scan rate for **a** CT/GCE electrode; **b** Nano-MnO_2/CT/GCE; **c** ChOx Nano MnO_2/CT/GCE; and **d** nano-MnO_2/GCE bioelectrodes in phosphate buffer (50 mM, pH 7.0, 0.9 % NaCl) containing $[Fe(CN)6]^{3-/4-}$ (5 mM) at 10–100 mV s^{-1} (from *inner* to *outer*)

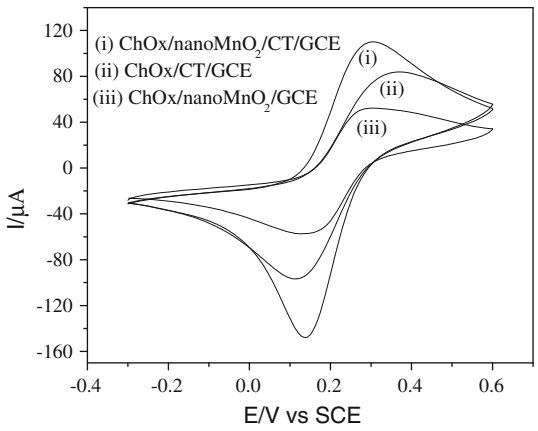

Fig. 7 CVs of *i* ChOx/nanoMnO$_2$/CT/GCE; *ii* ChOx/CT/GCE; and *iii* ChOx/NanoMnO$_2$/GCE with 11.66 mM cholesterol at scan rate 50 mV s^{-1} and other conditions similar to Fig. 6

nano-MnO$_2$/CT electrode in PBS (50 mM, pH 7.0, 0.9 % NaCl) containing $[Fe(CN)_6]^{3-/4-}$(5.0 mM) were recorded as a function of scan rate (10–100 mV s^{-1}) [Fig. 6a(i), b(i)]. Both the cathodic (I_{pc}) and anodic peak currents (I_{pa}) of the modified electrodes increased linearly with scan rate [Fig. 6a(ii), b(ii)]. We performed CV experiments for nano-MnO$_2$/CT/GCE (without ChO$_x$). But, no specific sensing signal was observed.

After adsorption of the ChOx onto nano-MnO$_2$/CT/GCE bioelectrode, reversible electron transfer was possible [Fig. 6c(i)]. Redox peak currents were found to be proportional to the square root of scan rate [Fig. 6c(ii)]. Linear dependence of peak currents and scan rate suggested diffusion-controlled process. With incorporation of nano-MnO$_2$ (nano-MnO$_2$/CT) in CT film, redox potential shifted toward the high side [Fig. 6b(i)]. Modified bioelectrode provided biocompatible micro-environment for ChOx enzyme, and accelerated the electron transfer because of strong interactions [35]. CV curves of ChOx/nano-MnO$_2$/CT/GCE with cholesterol (11.66 mM) showed higher current and less anodic potential in compare with ChOx/CT/GCE and thus suitable for cholesterol detection (Fig. 7).

The surface concentration of nano-MnO$_2$/CT/GCE bioelectrode was estimated by CV curves using Brown-Anson model [36].

$$I_p = \frac{n^2F^2\gamma AV}{4RT} \quad (2)$$

In Eq. (2), n is the number of electrons transferred at electrode, F is the Faraday constant (96,485 C mol^{-1}), γ is the surface concentration of the modified bioelectrode (mol cm^{-2}), A is the electrode surface area (7.07 mm^2), V is the scan rate (30 mV s^{-1}), R is the gas constant (8.314 J mol^{-1} K^{-1}), and T is the absolute temperature (298 K). In Eq. (2), peak current (I_p) and surface concentration (γ) are linearly proportional. Peak current increased due to enhanced interaction between analyte and modified electrode surface. Hence, high surface concentration of the modified bioelectrodes confirmed strong interaction between analyte and modified electrode surface. Surface concentration values for nano-MnO$_2$/CT/GCE (5.01×10^{-11} mol cm^{-2}) and ChOx/nano-MnO$_2$/CT/GCE electrodes (2.404×10^{-8} mol cm^{-2}) confirmed strong interaction (between ChOx and nano-MnO$_2$/CT/GCE), and enhanced electron transport.

The effect of pH on ChOx/nano-MnO$_2$/CT/GCE bioelectrode was also studied by CV at 50 mV s^{-1} scan rate and room temperature (Fig. 8a). Relatively high current response for the modified bioelectrode at pH: 7.0 indicated high activity of ChOx/nano-MnO$_2$/CT/GCE bioelectrode (Fig. 8b). Under these conditions (physiological pH: 7.0), ChOx retained its natural structure without any denaturation [27]. Thus, all experiments were done at pH: 7.0 and 25 °C.

Electrochemical oxidation of cholesterol (0.03–11.66 mM) on ChOx/CT/GCE and ChOx/nano-MnO$_2$/CT/GCE electrode was studied by CV [Fig. 9a(i), b(i)] under identical experimental conditions (in 50 mM PBS; pH 7.0; 0.9 % NaCl containing 5 mM $[Fe(CN)_6]^{-3/-4}$). Magnitude of the response

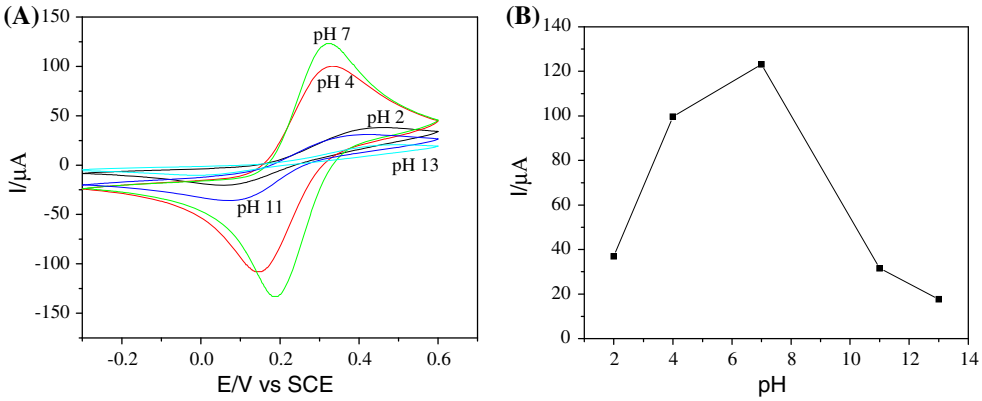

Fig. 8 **a** CVs of ChOx/NanoMnO$_2$/CT/GCE bioelectrode in different pH ranges with 1.29 mM cholesterol, **b** dependence of the modified bioelectrode with the pH of electrolyte solution at scan rate 50 mV s^{-1} and other condition similar to Fig. 6

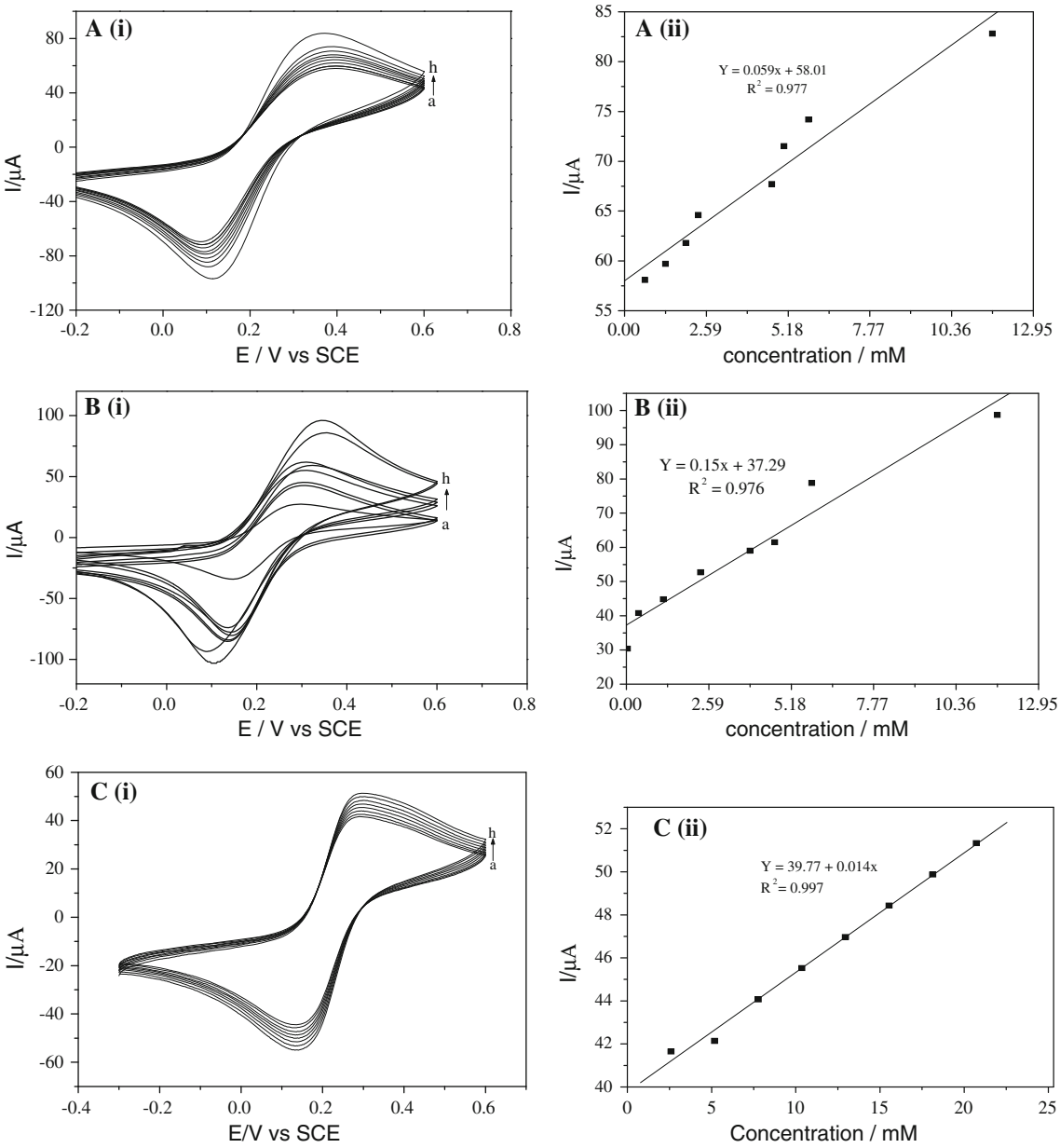

Fig. 9 CVs of **a** *i* ChOx/CT/GCE with different concentrations (0.64–11.66 mM); **b** *i* ChOx/NanoMnO$_2$/CT/GCE with different concentrations (0.03–11.66 mM); **c** *i* ChOx/nano-MnO2/GCE with different concentrations (0.64–11.66 mM); and *ii* represents the relationship between the current and different concentration of cholesterol at scan rate 50 mV s^{-1} and other condition similar to Fig. 6

current rapidly increased with cholesterol concentration [Fig. 9a(ii), b(ii)]. This was attributed to the presence of ChOx on the CT/GCE and nano-MnO$_2$/CT/GCE bioelectrodes. During the oxidation, cholesterol converted into cholesterone (choleste-4-ene-3-one) and liberated the electrons. These electrons were transferred to the CT/GCE or to the nano-MnO$_2$/CT/GCE via mediator (Fe^{+3}/Fe^{+4} redox couple) and enhanced the charge transfer thus exhibited high sensitivity [23]. Proposed biochemical reactions during the cholesterol oxidation are depicted in Scheme 1. High sensitivity of ChOx/nano-MnO$_2$/CT/GCE bioelectrode was observed due to well-aligned close-packed arrangement of nano-MnO$_2$. Formation of hydrogen bonds between MnO$_2$ and CT was responsible for biocompatibility of modified electrode for ChOx. In 0.64–11.66 mM concentration range of cholesterol, ChOx/CT/GCE showed good linearity [Fig. 9a(ii)] and sensitivity 2.28 μA mM^{-1} ($R^2 = 0.977$), while cholesterol showed linearity over 0.03–11.66 mM concentration range on ChOx/nano-MnO$_2$/CT/GCE [Fig. 9b(ii)] with 5.59 μA mM^{-1} sensitivity ($R^2 = 0.976$). To determine the LOD value for the proposed biosensor, we prepared analyte solutions with low concentrations (2.59×10^{-4}–5.18×10^{-2} mM).

Electrochemical response of the ChOx/nano-MnO_2/CT/GCE modified electrode was studied by CV by adding these analyte solutions separately in PBS (50 mM, pH 7.0, 0.9 % NaCl) containing 5 mM $[Fe(CN)6^{-3/-4}]$. Modified bioelectrode showed good response and accuracy for the analyte solution with 2.07×10^{-3} mM concentration. Thus, LOD of the reported biosensor was estimated as 2.07×10^{-3} mM (S/N = 3) by three repeated measurements.

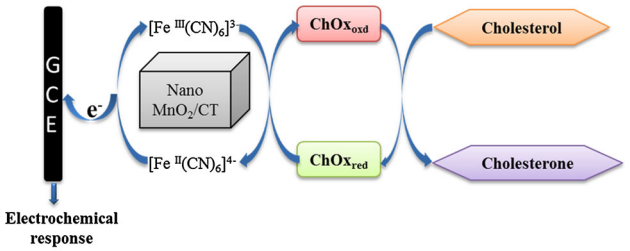

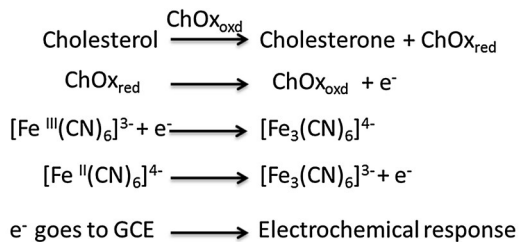

Scheme 1 Schematic presentation and biochemical reactions during oxidation of cholesterol at ChOx/nano-MnO_2/CT modified GCE

3.4 Amperometric biosensing of cholesterol

To study the performance of ChOx/nano-MnO_2/CT/GCE bioelectrode, amperometric measurements were performed at different cholesterol concentrations in 50 ml PBS (50 mM, pH 7.0, 0.9 % NaCl) containing 5.0 mM $[Fe(CN)_6]^{3-/4-}$. With successive step-wise cholesterol addition under stirred condition (100 rpm), well-defined, stable, and fast amperometric responses were observed at 0.4 V (Fig. 10a). Current response for the modified electrode increased in steady manner with progressive cholesterol addition. Reported sensor showed fast response within 5 s, and attended steady-state value (95 %). Calibration curves for the modified electrode (with a linear regression coefficient of 0.998) are included in Fig. 10b. High sensitivity of ChOx/nano-MnO_2/CT/GCE sensor with good

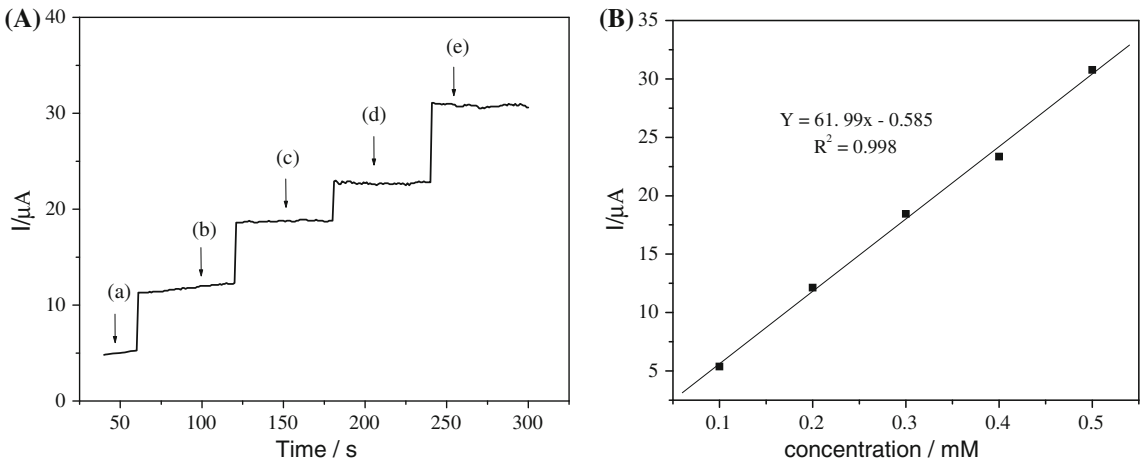

Fig. 10 **a** Amperometric response of ChOx/nano MnO_2-CT/GCE with successive addition of 0.1 ml cholesterol in 50 mM PBS (50 ml) at 400 mV: **a** 0.1 mM, **b** 0.2 mM, **c** 0.3 mM, **d** 0.4 mM, and **e** 0.5 mM of cholesterol at 60 s interval. **b** Calibration plot of I vs cholesterol concentration (obtained from chronoamperometric experiment)

Table 1 Comparison of analytical performance of CT-based cholesterol biosensors reported literature

Electrode	Sensitivity ($\mu A\ mM^{-1}\ cm^{-2}$)	Linearity (mM)	LOD (mM)	Stability (days)	References
ChOx/CT/ZnO/ITO	5,444.0	0.13–7.77	0.130	85	[4]
ChOx/CT/AuPt/IL/GCE	90.7	0.05–6.20	0.010	–	[26]
ChOx/CT/CeO_2/ITO	1,814.6	0.23–10.36	0.130	60	[7]
ChOx/CT/NiO/ITO	31.2	0.23–10.36	1.120	70	[23]
ChOx/CT/SnO_2/ITO	1,339.7	0.23–10.36	0.130	90	[27]
ChOx/CT/SiO_2/MWNT/ITO	0.1	1.29–16.83	1.230	180	[25]
ChOx/CT/SiO_2/MWCNTs/PB/GCE	0.5	0.008–45.00	0.004	50	[37]
ChOx/CT/MnO_2/GCE	5.6	0.03–11.66	0.002	90	This work

LOD and fast response time was attributed to the well-aligned and closed packed network of nano-MnO_2 which acted as a good electron acceptor and enhanced the electrocatalytic active areas responsible for promotion of electron transfer during cholesterol oxidation.

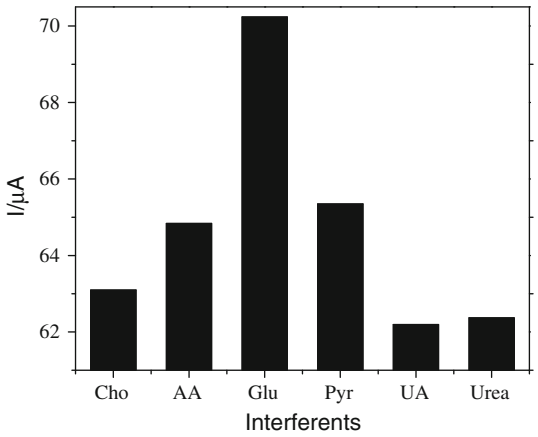

Fig. 11 Effect on of interferents on ChOx/NanoMnO$_2$/CT/GCE bioelectrode during cholesterol estimation

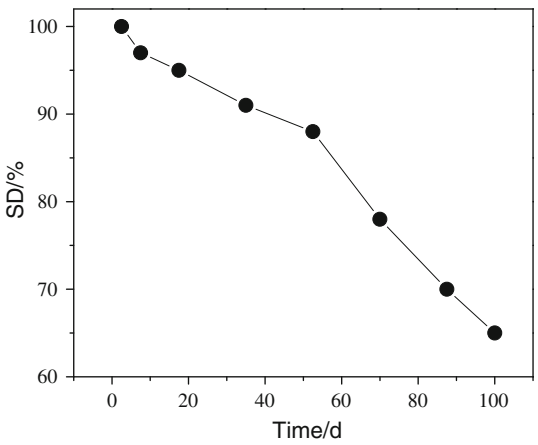

Fig. 12 Stability test of modified bioelectrode

Table 1 summarizes characteristics of ChOx/nano-MnO_2/CT/GCE biosensor along with other ChOx/metal oxides/CT biosensors. Data indicated that nano-MnO_2 not only affects the catalytic property of ChO_x but also improves storage stability, LOD, linearity, and sensitivity. These demonstrated the efficiency of ChOx/nano-MnO_2/CT/GCE biosensor as a new transducer element for cholesterol-sensing platform.

3.5 Selectivity and stability

In biological samples, ascorbic acid, glucose, urea, lactic acid, and pyruvic acid interfere during the selective cholesterol detection. Under optimized conditions, selectivity of ChOx/nano-MnO_2/CT/GCE bioelectrode was estimated by magnitude of response current by addition of interferents [glucose (5 mM), ascorbic acid (0.05 mM), uric acid (0.1 mM), urea (5 mM), and pyruvic acid (5 mM)]. Interferents altered $\sim$2–7 % in peak current (Fig. 11). Selectivity of ChOx/nano-MnO_2/CT/GCE bioelectrode was nearly unaffected due to the presence of interferents.

The reproducibility of ChOx/NanoMnO$_2$/CT/GCE bioelectrode for detection of cholesterol was investigated by CV peak current response recorded ten times. Measured values showed 1.1 % RSD value for 0.03 mM cholesterol concentration. Under this condition, the oxidation current for cholesterol was almost unchanged (decreased about $>$1.7 %) between -0.3 and 0.6 V potential in 0.2 M phosphate buffer solution (50 mM, pH 7.0, 0.9 % NaCl) containing 5 mM $[Fe(CN)_6]^{3-/4-}$) at 50 mV s^{-1} scan rate during 200 cycles. To assess the shelf-life of ChOx/nano-MnO_2/CT/GCE bioelectrode, it was stored at 4 °C temperature in PBS, and no significant alteration in current response was recorded for cholesterol detection after 3 months (Fig. 12). Biosensing characteristics of the ChOx/nano-MnO_2/CT/GCE bioelectrode were compared

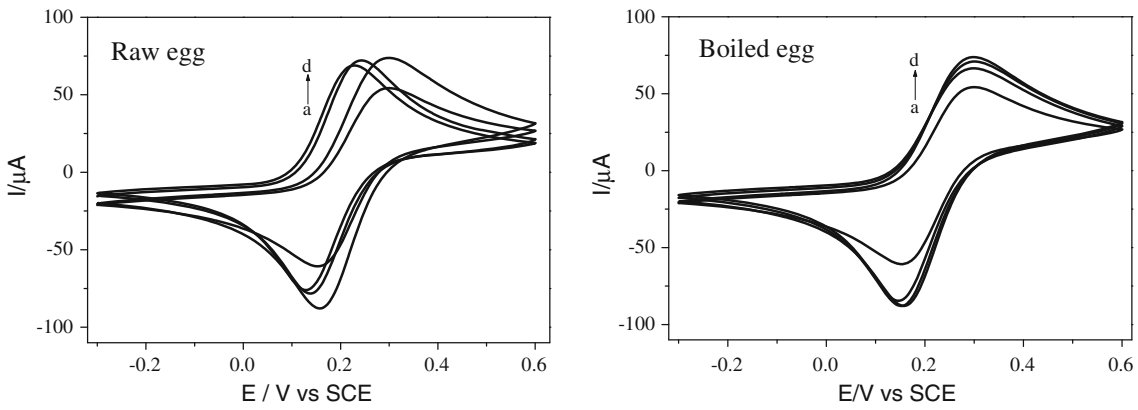

Fig. 13 CVs of egg in food samples at scan rate 50 mV s^{-1} and other condition similar to Fig. 6

with other electrodes based on metal oxide nanoparticles available in the literature (Table 1) [4, 23, 25–27, 37].

3.6 Real samples detection

Validity of the developed sensor was also assessed by monitoring the cholesterol concentration in food samples. Raw egg yolk (47.05 g) and boiled egg yolk (7.5 g) were dispersed in 10 % triton X-100 solution separately. 5 ml of this sample solution was added in 25 ml of phosphate buffer solution (50 mM, pH 7.0, 0.9 % NaCl containing 5 mM $[Fe(CN)_6]^{3-}/^{4-}$) and CV was recorded at 50 mV s^{-1} scan rate (Fig. 13). Obtained response currents 48.8 μA (a), 63.8 μA (b), 67.8 μA (c), and 69.3 μA (d) corresponded to 1.8, 4.7, 5.3, and 5.6 cholesterol concentrations for raw eggs. In case of boiled eggs, response currents 51.8 μA (a), 60.8 μA (b), 65.8 μA (c), and 69.8 μA (d) corresponded to 2.5, 4.0, 4.9, and 5.6 cholesterol concentrations. Total cholesterol concentration measured in boiled egg and raw egg was quite similar with the earlier reported result [38]. Further, it was observed that cholesterol concentration was increased after cooking, may be due to the retention and tissue moisture losses.

4 Conclusions

In summary, nano-MnO_2 provides conformational environment for ChOx loading and electron between ChOx and modified electrode surface. Reported bioelectrode with 0.03–11.66 mM linearity, 2.07×10^{-3} mM LOD, 5.59 μA mM^{-1} sensitivity, and 0.976 regression coefficient value (R^2) showed 3 months shelf-life. Efforts were attempted to utilize ChOx/nano-MnO_2/CT/GCE bioelectrode for quantitative estimation of cholesterol concentration in food samples. Reported bioelectrode provides a new class of sensing platform for cholesterol detection.

Acknowledgments Authors are thankful to Department of Science and Technology (DST) for financial support by sponsoring project no. DST/TSG/ME/2010/57. We also acknowledge the services of analytical science division, CSMCRI, Bhavnagar for instrumental support.

References

1. Baynes JW, Dominiczak M (2005) Medical biochemistry, 2nd edn. Elsevier, Amsterdam
2. White A, Handler P, Smith EL, Hill RL, Lehman IR (1987) Principles of biochemistry, 6th edn. McGraw-Hill Book, New York, pp 903–907
3. Kumar A, Pandey RR, Brantley B (2006) Talanta 69:700–705
4. Khan R, Kaushik A, Solanki PR, Ansari AA, Pandey MK, Malhotra BD (2008) Anal Chim Acta 616:207–213
5. Ansari AA, Kaushik A, Solanki PR, Malhotra BD (2008) Electrochem Commun 10:1246–1249
6. Singh SP, Arya SK, Pandey P, Malhotra BD, Saha S, Sreenivas K, Gupta V (2007) Appl Phys Lett 91:063901–063903
7. Malhotra BD, Kaushik A (2009) Thin Solid Films 518:614–620
8. Jiang HL, Kwon JT, Kim YK, Kim EM, Arote R, Jeong HJ, Nah JW, Choi YJ, Akaike T, Cho MH, Cho CS (2007) Gene Ther 14:1389–1398
9. Liao JD, Lin SP, Wu YT (2005) Biomacromolecules 6:392–399
10. Suib SL (2008) Acc Chem Res 41:479–487
11. Kuo C-C, Lan W-J, Chen C-H (2014) Nanoscale 6:334–341
12. Liu A (2008) Biosens Bioelectron 24:167–177
13. Zhai T, Fang X, Liao M, Xu X, Zeng H, Yoshio B, Golberg D (2009) Sensors 9:6504–6529
14. Huang J, Wan Q (2009) Sensors 9:9903–9924
15. Ahammad AJS, Lee JJ, Rahman MA (2009) Sensors 9:2289–2319
16. Kaushik A, Khan R, Solanki PR, Pandey P, Ahmad S, Malhotra BD (2008) Biosens Bioelectron 24:676–683
17. Wei H, Wang E (2008) Anal Chem 80:2250–2254
18. Jia NQ, Zhou Q, Liu L, Yan MM, Jiang ZY (2005) J Electroanal Chem 580:213–221
19. Yu J, Ju H (2002) Anal Chem 74:3579–3583
20. Kim HJ, Yoon SH, Choi HN, Lyu YK, Lee WY (2006) Bull Korean Chem Soc 27:65–70
21. Ansari AA, Solanki PR, Malhotra BD (2008) Appl Phys Lett 92:263901–263903
22. Mehta A, Patil S, Bang H, Cho HJ, Seal S (2007) Sens Actuators. A 134:146–151
23. Singh J, Kalita P, Singh MK, Malhotra BD (2011) Appl Phys Lett 98:123702–123703
24. Tsai YC, Chen SY, Lee CA (2008) Sens Actuators. B Chem 135:96–101
25. Tiwari A, Gong S (2008) Electroanalysis 20:2119–2126
26. Safavi A, Farjami F (2011) Biosens Bioelectro 26:2547–2552
27. Ansari AA, Kaushik A, Solanki PR, Malhotra BD (2009) Electroanalysis 21:965–972
28. Kaushik A, Solanki PR, Kaneto K, Kim CG, Ahmad S, Malhotra BD (2010) Electroanalysis 22:1045–1055
29. Norouzi P, Faridbod F, Nasli-Esfahani E, Larijani B, Ganjali MR (2010) Int J Electrochem Sci 5:1008–1017
30. Report of the National Cholesterol Education Program Expert Panel on detection, evaluation, and treatment of high blood cholesterol in adults (1988). Arch Intern Med 148:36–69
31. Choi SH, Lee SD, Shin JH, Ha J, Nam H, Cha GS (2002) Anal Chim Acta 461:251–260
32. Zhu S, Zhou H, Hibino M, Honma I, Ichihara M (2005) Adv Funct Mater 15:381–386
33. Khan R, Dhayal M (2008) Electrochem Commun 10:263–267
34. Wang X, Li Y (2003) Chem Eur J 9:300–306
35. Zhang HL, Zou XZ, Lai GS, Han DY, Wang F (2007) Electroanalysis 19:1869–1874
36. Bard AJ, Faulkner LR (2000) Electrochemical methods: fundamentals and applications, 2nd edn. Wiley, New York
37. Tan X, Li M, Cai P, Luo L, Zou X (2005) Anal Biochem 337:111–120
38. Basu A, Chattopadhyay P, Roychoudhuri U, Chakraborty R (2007) Bioelectrochemistry 70:375–379